Acoustic waveform of continuous bubbling in a non-Newtonian fluid

Valérie Vidal,[1,*] Mie Ichihara,[2] Maurizio Ripepe,[3] and Kei Kurita[2]
[1]*Université de Lyon, Ecole Normale Supérieure, CNRS, 46 Allée d'Italie, 69364 Lyon Cedex 07, France*
[2]*Earthquake Research Institute, University of Tokyo, 1-1-1 Yayoi, Bunkyo-ku, Tokyo 113-0032, Japan*
[3]*Dipartimento di Scienze della Terra, Università degli Studi di Firenze, Via La Pira 4, 50121 Firenze, Italy*
(Received 15 June 2009; revised manuscript received 5 November 2009; published 23 December 2009)

We study experimentally the acoustic signal associated with a continuous bubble bursting at the free surface of a non-Newtonian fluid. Due to the fluid rheological properties, the bubble shape is elongated, and, when bursting at the free surface, acts as a resonator. For a given fluid concentration, at constant flow rate, repetitive bubble bursting occurs at the surface. We report a modulation pattern of the acoustic waveform through time. Moreover, we point out the existence of a precursor acoustic signal, recorded on the microphone array, previous to each bursting. The time delay between this precursor and the bursting signal is well correlated with the bursting signal frequency content. Their joint modulation through time is driven by the fluid rheology, which strongly depends on the presence of small satellite bubbles trapped in the fluid due to the yield stress.

DOI: 10.1103/PhysRevE.80.066314 PACS number(s): 47.50.−d, 43.20.+g, 83.60.Rs, 91.40.−k

I. INTRODUCTION

Many repetitive signals can be found in nature, from everyday's life to larger-scale natural phenomena. For instance, the typical "pop" sound of poured soda or champagne, the bubbling of sauce cooking in the kitchen [1], geyser quasiperiodic activity [2], volcanic explosions [3–5] or ground deformation [6–8], seismic swarms [8], or even "seismic raves," observed during dance festivals [9]. The analysis of the acoustic signal produced by such systems represents, when possible, a nonintrusive way to investigate the origin, the characteristics and the occurrence of these events.

Among these systems, we will focus on the repetitive sound produced by successive bubble burstings. At the laboratory scale, foamy systems have received a special attention during the last decade, as paradigms for disordered materials [10–15]. In collapsing foams, bubbles burst in cascades or avalanches, generating acoustic signals. The frequency of the bubble rupture slowly evolves with time [10], and the frequency of the acoustic signal itself is shown to be statistically correlated with the typical bubble size [12,15]. At large scale, giant gas bubbles bursting on volcanoes provide a natural example of sound generation. By decompression during the magma ascent in the volcanic conduit, bubbles form, coalesce, rise, then burst at the surface of lava lakes or at the volcanic vent [7,16], generating quasiperiodic acoustic signals [3–5], whose spectral content can change from one event to the other [5]. The two examples above point out the fact that on the one hand, the occurrence of repetitive signals is not necessarily periodic; on the other hand, the signal content itself can vary from one event to the other. Understanding the mechanisms controlling not only the characteristic periodicity of the events, but also the deviation from this periodicity and the temporal evolution of the signal content, is scientifically interesting, and might be of importance for practical reason, as mitigation of natural disasters.

Most of the fluids involved in these processes are non-Newtonian fluids, whose complex rheological properties are responsible for a flow behavior different from Newtonian fluids [17]. Compared to the present knowledge of bubbles in Newtonian solutions, the study of bubble behavior—and in particular, bubble bursting—in non-Newtonian fluids still remains at an elementary stage. In a recent work, the acoustics of a single bubble bursting at the free surface of a non-Newtonian fluid has been studied extensively [18]. Due to the viscoelastic gel properties, the bubble shape is generally elongated [17,19–21], and the bubble walls do not deform during the acoustic emission at bursting. Consequently, triggered by the film bursting, the bubble body acts as a resonator, and the acoustic signal frequency can be directly linked to the bubble length and shape. Experiments investigating the resonance of a cavity of well-controlled geometry, triggered by a thin-film bursting [22], identified the physical processes at stake in the generation, propagation, radiation, and damping of the acoustic signal.

Here, we present the analysis of the acoustic waveform produced by repetitive bubble burstings at the free surface of a non-Newtonian fluid column, at the bottom of which air is injected at constant flow rate. The formation and rise of bubbles in such a system and, in particular, the in-line interaction of the rising bubbles, have been studied in details [23–26], including the departure from the periodic behavior [27]. In our study, we focus on the bubble bursting and, in particular, on the variations in the acoustic waveform through time, while the bubbles burst quasiperiodically at the free surface. We observe a surprisingly systematic pattern in the modulation of the acoustic waveform through time (Sec. III A). We point out the existence of a precursor acoustic signal. The time delay between this precursor and the bursting event forecasts the subsequent change of the bursting signal spectral content (Sec. III B). Finally, we propose mechanisms to explain the waveform, the precursor generation, and the signal modulation (Sec. IV).

II. EXPERIMENTAL SETUP

The experimental setup (Fig. 1) consists of a plexiglas cell 100 mm height, of internal circular cross section (radius of 25 mm) and external square cross section (90×90 mm^2).

*valerie.vidal@ens-lyon.fr

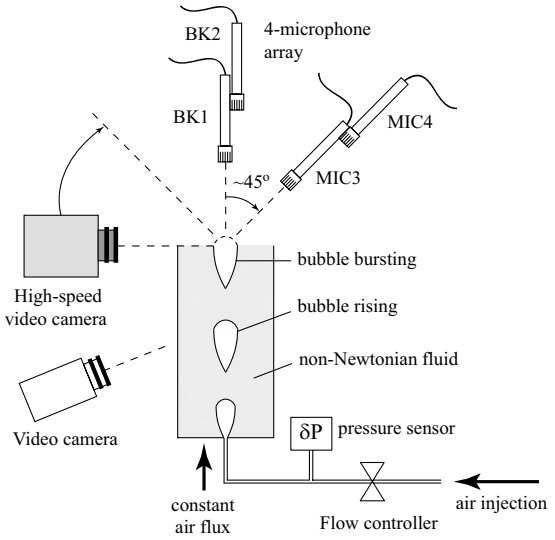

FIG. 1. Experimental setup. Microphones are located at a distance of $d=3$ or 10 cm from the fluid free surface, and an angle $\alpha=0°$ or 45° from the vertical. δP is the overpressure at the bottom of the fluid column.

The cell is filled up to its upper plane by a non-Newtonian fluid consisting of a commercial hair-dressing gel (GATSBY SH Styling Gel, Mandom Corp.), diluted in distilled water. The choice of such fluid is justified by the fact that the mixtures are easily reproducible and very stable in the time [26]. In order to avoid any changes due to the gel aging, experiments are performed in the same fluid for not more than a week. Over this time period, no significant change of the fluid rheological properties due to aging is observed. The non-Newtonian fluid characteristics can easily be tuned by changing the percentage of dilution of the gel in water. In the following sections, all dilutions indicated are given in weight percentage of the gel in the mixture. Due to the fluid yield stress, the mixture is initially filled with small trapped bubbles (*bubbly gel*) [28]. In order to investigate the effect of these background bubbles, for some series of experiments (see Sec. IV C), we have removed the trapped bubbles either by successive decompression and compression of the fluid, or by centrifuge (*pure gel*). Air is supplied from a pressure chamber to the cell bottom through a 2.5 mm hole, at constant flow rate, by means of a regulator valve (Swagelok SS-SS2-D-VH). A pressure sensor (KISTLER 701A) and a pressure gauge (Keyence AP-C30) record the pressure variations in the injection pipe and in the pressure chamber, respectively. Due to constant air injection, bubbles continuously form, rise, and then burst at the free surface of the non-Newtonian fluid. Unless specified, the data presented in the figures are for a 60% gel solution, and a flow rate of 0.7 mL s^{-1}.

The acoustic signal associated with the successive bubble burstings is recorded by a four-microphone array (see Fig. 1), consisting of two audio microphones (MIC3 and MIC4: ECZ-990, Azden Corp.), and two broadband condenser microphones (BK1 and BK2: Bruel & Kjaër 4193 microphones with a NEXUS 2690 signal conditioner). The BK microphones have a flat response in the range of 0.1 Hz–20 kHz, and their signals are used for waveform analyses. The MIC microphones are useful to detect the arrival time of each signal. All the signals are recorded at 200 kHz sampling rate. The microphones are located at a distance $d=3$ and 10 cm from the fluid surface, at an angle of 0° and 45° from the vertical (Fig. 1). The position of the microphones is chosen so that the closest microphones ($d=3$ cm) register both the acoustic signal and the jet wave (see Sec. III A) emitted by the bubble bursting; the farthest microphones ($d=10$ cm) record the acoustic wave only.

Bubbles rising up the gel column and bursting at the free surface are monitored by a video camera (SONY Handycam DCR-TRV900) at 30 frames/s. Simultaneous acquisition of the video and acoustics is performed by a data acquisition system (DEWE-5000). In addition, a high-speed video camera (Photoron FASTCAM-1024PCI), synchronized with the microphone acquisition system, has been used to record images up to 7500 frames/s either from the side, or from above the fluid surface.

III. ACOUSTIC WAVEFORM

In this section, we investigate the shape of the acoustic waveform at bursting (Sec. III A), and the existence of another, smaller-amplitude acoustic signal, previous to bursting (Sec. III B).

A. Signal at bursting

We record the acoustic signal produced by the successive bubbles bursting at the non-Newtonian fluid free surface. Figure 2(a) displays part of a typical time series, in which we continuously recorded up to 248 bursting events. Each peak in the signal corresponds to a bubble bursting at the free surface of the fluid, which occurs quasiperiodically. The acoustic signal associated with the bursting, which is the target of this study, is the beginning high-frequency oscillation recorded by all the microphones coherently [Figs. 2(b)–2(e)]. The closer microphones (BK1 and MIC3, located at $d=3$ cm, see Fig. 1) recorded strong low-frequency signals starting either right after or slightly superimposed to the end of the acoustic signal [Figs. 2(b) and 2(c), indicated as *jet*]. This signal is not an acoustic wave, but the dynamic pressure associated with the advection of air released out of the overpressurized bubble, which velocity of propagation is of the order of a few tens of meters per second. This velocity is estimated either by measuring the time delay between the bubble head opening and the time arrival of the jet signal at the closest microphones or, for a few experiments, by measuring the jet wave arrival time at two microphones located close to the free surface ($d=1.5$ and 3 cm). In the following waveform analyses, the jet component is eliminated by a curve fitting (fourth order polynomial).

Inside the same continuous bubbling series, the acoustic signals associated with bubble bursting at the fluid surface exhibit very different waveforms. Figure 3 displays the example of a series of 20 successive bursting events (events #191 to #210). The acoustic signals vary between a *resonant-type* waveform [e.g., Figure 3(b), event #193] and a *blast-*

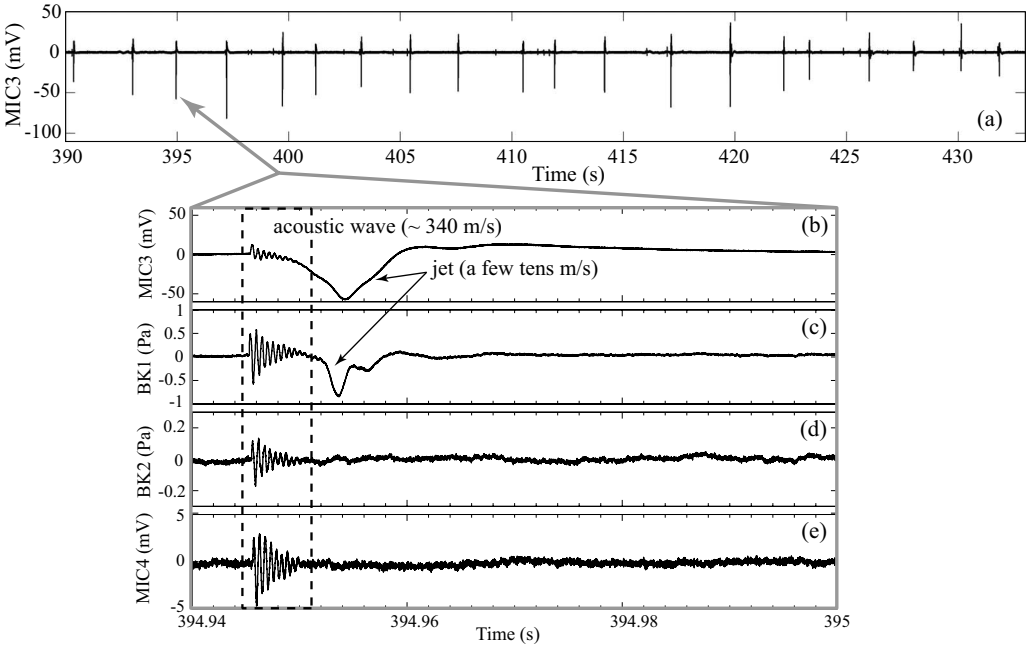

FIG. 2. (a) Example of continuous acoustic signal recording. Each peak in the acoustic signal indicates a bubble bursting at the fluid free surface. (b,c,d,e) Zoom on a bursting signal, recorded by the microphones MIC3 (b), BK1 (c), BK2 (d), and MIC4 (e). Note the acoustic waveform (delimited by the dashed vertical lines), followed by the jet wave for the nearest microphones (MIC3 and BK1, see text). (See Fig. 1 for the microphones location.)

type waveform [e.g., Figure 3(c), event #201]. The spectral content of the two signals are quite different both in the location of the peaks (arrows with numbers in kHz) and the general slope (dashed gray line) [see Figs. 3(b) and 3(c)]. The peaks represent the characteristic resonance frequencies inside a cavity, while the slope represents the weakening of the higher-frequency modes respect to the lower-frequency modes.

A resonant-type signal is characterized by the dominance of the lowest mode. This waveform has been reported in the literature [18] that investigated a single isolated bubble bursting at the free surface of a similar non-Newtonian fluid.

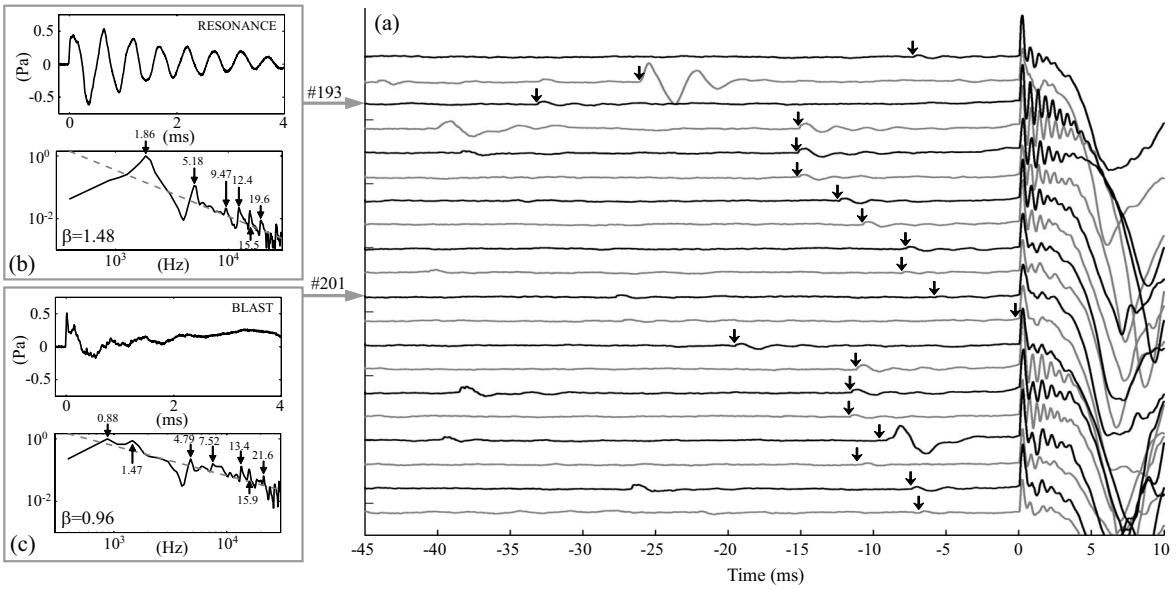

FIG. 3. Example of 20 successive bursting events. (a) Signal recorded by microphone MIC3 (jet contribution not removed). On the right-hand part, the acoustic waveform associated with the bursting changes through time. Previous to the bursting, note the existence of a precursor acoustic signal (black arrows). The time-delay Δt_{prec} between the precursor and the acoustic signal associated with bubble bursting varies from one explosion to the other. (b,c) Zoom on (b) a resonant-type waveform (event #193) and (c) a blast-type waveform (event #201), with their associated spectrum. Arrows and numbers indicate the frequency peaks, in kHz. The dashed gray line displays the general slope β of the spectrum.

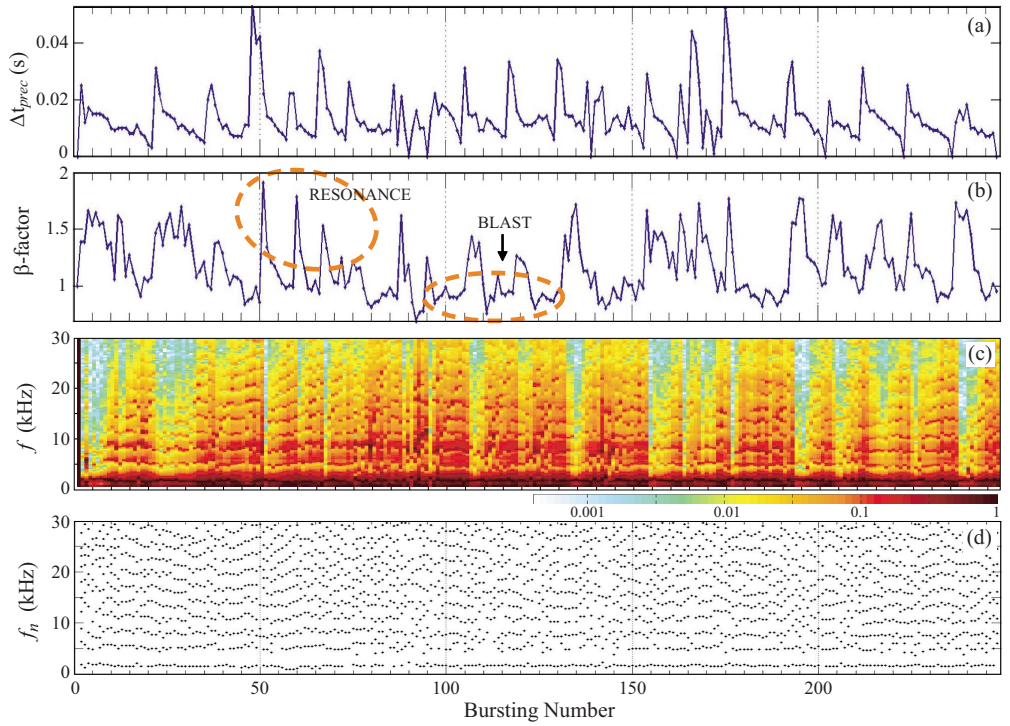

FIG. 4. (Color online) Analysis of the precursor signal. (a) Time-delay Δt_{prec} between the precursor and the acoustic signal associated with bubble bursting, as a function of the bursting event. (b) β factor (spectrum slope, see insets Figs. 3(c) and 3(d)). (c) Normalized log-spectrogram of the bursting events, filtered between 0.78 and 29.9 kHz. (d) Frequency peaks of the spectrum as a function of the bursting event.

The authors showed that the dominant frequency of the wave is directly linked to the fundamental resonance mode of the open cavity. The frequency is determined by the length and shape of the bubble, and the excitation of the acoustic resonance strongly depends on the characteristic rupture time of the film [18]. In the case of a blast-type signal, the spectrum exhibits higher frequency modes. In our experiment, all the intermediate waveforms between these two extreme types are observed.

In order to quantify the waveform characteristics, we define a parameter β by fitting the spectrum amplitude by

$$A = \xi f^{-\beta}, \tag{1}$$

where β represents the spectrum slope. As an example, in Fig. 3, we estimate the spectrum slope for the resonant-type signal β=1.48 [Fig. 3(b)], whereas for the blast-type signal β=0.96 [Fig. 3(c)].

B. Precursor signal and modulation pattern

For almost all bursting events, previous to the signal associated with bursting, we record a *precursor* acoustic signal. We pick the arrival time of the precursor signal nearest to the bubble bursting (Fig. 3, black arrows). The time-delay Δt_{prec} between this precursor and the acoustic signal associated with the bursting itself varies strongly during a continuous series. Moreover, this variation seems correlated with the bursting acoustic waveform. In order to investigate this feature, we have performed a systematic analysis of the time-delay Δt_{prec}, and the spectrum associated with the bursting event, for a time series of 248 bursting events (see Fig. 4). For each bursting, we calculate the time-delay Δt_{prec} between the precursor and the acoustic signal [Fig. 4(a)], and the exponent β from Eq. (1) [Fig. 4(b)]. In order to represent the time evolution of the bursting signal spectral content, we display in Fig. 4(c) the spectrogram of the acoustic waveform, as a function of the bursting event number. Finally, Fig. 4(d) shows the temporal evolution of the peak frequencies, picked as in Figs. 3(b) and 3(c).

A joint variation in Δt_{prec}, β and the spectral content as a function of time (or bursting event) is clearly visible in Figs. 4(a)–4(c). From small values of both Δt_{prec} and β (blast-type waveform), the system switches quickly to a large Δt_{prec} and a large β exponent (resonant-type waveform). Right after the maximum in Δt_{prec}, the acoustic waveform becomes strongly resonant. Then both Δt_{prec} and β lead back to the blast-type acoustic signal events [small Δt_{prec} and small β, Figs. 4(a) and 4(b)]. This feature is repeated through the bursting history. Hereafter, we will refer to this pattern as *modulation pattern*. Note that a slow gliding of the higher harmonic frequencies upward also occurs [Fig. 4(d)], but the correlation of the precursor time delay to the spectral peaks is not as clear as that to the β factor.

In order to quantify the correlation between Δt_{prec} and β, we represented in Fig. 5(a) the correlation between these parameters. It shows a clear peak with a lag that is not zero, but of one or two events. We attempted to plot β_n, β_{n+1}, and β_{n+2} against $\Delta t^n_{\mathrm{prec}}$, where n indicates the nth event (Fig. 6), but failed to see any clear correlation. The lack of correlation in Fig. 6 indicates that the correlation between β and Δt_{prec}

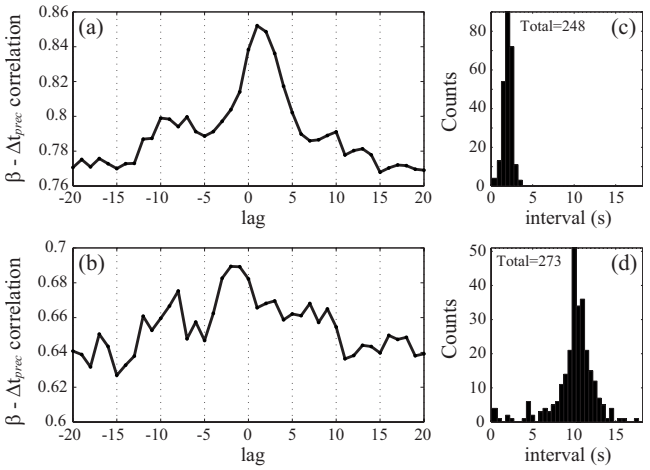

FIG. 5. Cross-correlation coefficients between Δt_{prec} and the β factor for (a) an air flow-rate of 0.7 mL s^{-1} (same data as Fig. 4) and (b) a smaller air-flow rate of 0.07 mL s^{-1}. The horizontal axis is the lag of the event number for the β factor from the one for Δt_{prec}. The distributions of the bursting intervals displayed in (c) and (d) correspond to (a) and (b), respectively.

is not one to one in magnitude. Nevertheless, according to Fig. 5, we confirm the existence of a correlation between Δt_{prec} and β, and that the peaks in β are delayed respect to the ones in Δt_{prec} by 1 or 2 events. We will comment on this in Sec. IV A.

IV. MECHANISMS

In this section, we discuss the mechanisms responsible for the observations reported above. In particular, we focus on the physical processes controlling the acoustic waveform (Sec. IV A) and the origin of the precursor signal (Sec. IV B), as well as the existence of the waveform modulation (Sec. IV C).

A. Waveform characteristics

When the bubble bursts at the free surface of the gel, the microphones record the acoustic signal subsequent to the film (bubble head) opening. The acoustic emission occurs over a time shorter than the time necessary for the bubble walls to collapse, or even to move significantly [18]. The bubble body is, therefore, regarded as an acoustic resonator, initially overpressurized, opened toward the atmosphere and

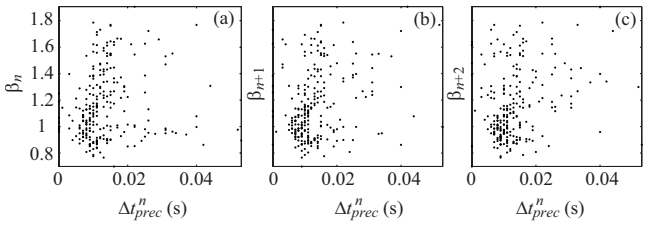

FIG. 6. β factor of (a) the nth, (b) the $(n+1)$th, and (c) the $(n+2)$th event, plotted as a function of the precursor time-delay $\Delta t^n_{\mathrm{prec}}$ of the nth event. Vertical scales are identical. No apparent correlation is found (see text).

excited by the film opening at bursting. The acoustic signal is thus determined both by the characteristic frequencies of the resonator, and by how the individual resonant modes are excited.

The characteristic frequencies of the acoustic wave inside the cavity formed by the bubble body at bursting are represented by the spectral peaks, as shown in Fig. 4(d). The fundamental frequency is in the range 1 to 2 kHz, for a bubble length of typically a few centimeters. Considering a cylindrical cavity of length $L \sim 5$ cm would give a fundamental resonant frequency of $f = c/4L \sim 1.7$ kHz; for a conical cavity having a cusp at its bottom, $f = c/2L \sim 3.4$ kHz. These estimated frequencies are higher than the fundamental frequency we find for the acoustic signal emitted by the blast-type and resonant-type bubbles [see spectra in Figs. 3(b) and 3(c)]. This lowering can be explained by the fact that the bubble head aperture is narrower than the bubble width itself, below the surface. Indeed, one-dimensional calculation of the resonating frequencies of a cavity taking into account a narrow aperture points out that the frequency lowers when the aperture gets narrower.

Here, the bubble shape is complex, and the estimation of the resonant frequencies associated with resonator shapes departing from the classical pipe or cone is non trivial [29,30] and out of the scope of this paper. Let us just remind that the characteristic frequencies of the acoustic wave are determined by the size and shape of the resonator [29–34]. The peak frequencies in Fig. 4(d) display no strong variation through time. Indeed, direct observations of the bubbles bursting in our experiment point out that the geometry of the bubble (length and general shape, see Fig. 9(b) for instance) does not change drastically from one bursting to another. It is noted that the change in geometry is likely to explain the small variations in the peak frequencies in time and, sometimes, the frequency gliding toward higher harmonics [Figs. 4(c) and 4(d)]. However, this process cannot account for the drastic change in the acoustic waveform, occurring for each modulation cycle, which is mainly associated with the spectral slope (β factor). Indeed, the systematic pattern in the waveform modulation [Fig. 4(c)] is better identified by the β factor [Fig. 4(b)] rather than the peak frequencies variations [Fig. 4(d)].

Figure 7 displays the dynamics of the bubble head opening, recorded by the high-speed video camera (7500 frames/s), for a resonant-type [Fig. 7(c), up] and a blast-type [Fig. 7(c), down] signal. The bubble bursting can be described as follows: a small hole forms on the bubble head, then grows until reaching its final size [Fig. 7(a)]. In Fig. 7(b), we report the evolution of the aperture radius as a function of time. We see a clear difference between the resonant- and blast-type signals. The analysis, repeated over a few experiments, shows this general tendency: the final opening size may vary, but for a resonant-type signal, over a time-scale on the order of 1 ms, the opening velocity is larger than for a blast-type signal. From another point of view, the opening seems to be saturated quicker for a blast-type signal than for a resonant-type signal. Although the time resolution of the observation is not enough to confirm the mechanism, it is inferred that the dominant mechanism responsible for the modulation is the film opening dynamics.

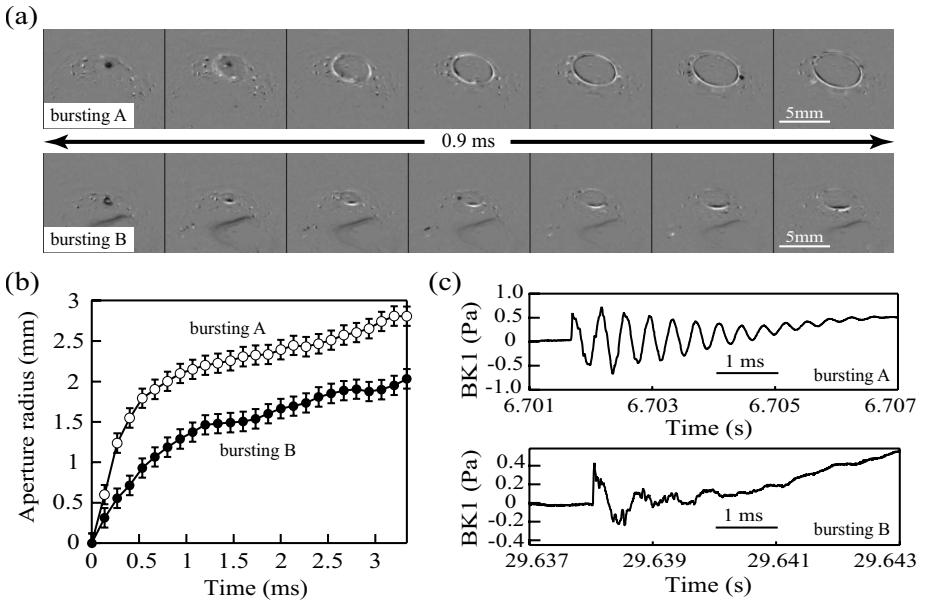

FIG. 7. Dynamics of the bubble head opening. (a) From left to right: images of the bubble opening taken with the high-speed video camera (7500 frames/s) for a resonant-type signal (up) and for a blast-type signal (down). In order to enhance the contrast, we display here the difference between two successive images. (b) Radius of the bubble head aperture as a function of time, for the resonant-type (open circles) and the blast-type (black circles) signals. (c) Resonant-type (up) and blast-type (down) acoustic signals corresponding to bursting A and B, respectively. Note that the total duration of the bubble head opening (about 0.9 ms) is only a small fraction of the acoustic signal duration.

B. Precursor generation

The mechanism responsible for the emission of a precursor acoustic signal has been investigated by imaging the bubble rising and bursting with the high-speed video camera (up to 7500 frames/s). This mechanism is summarized in Fig. 8. When a bubble with elongated shape bursts at the free surface of the non-Newtonian fluid, the bubble walls collapse quickly after the bubble head opening. As a consequence, a small satellite bubble is left behind, hereafter named *precursor bubble*. Due to the fluid yield stress, this small bubble remains trapped under the free surface [28]. As we are in a continuous bubbling regime, the following bubble, while rising, meets this remaining bubble and, eventually, they coalesce together (Fig. 8). This coalescence induces an acceleration of the fluid above the bubble—therefore, of the free surface—and, hence, generates the precursor acoustic signal.

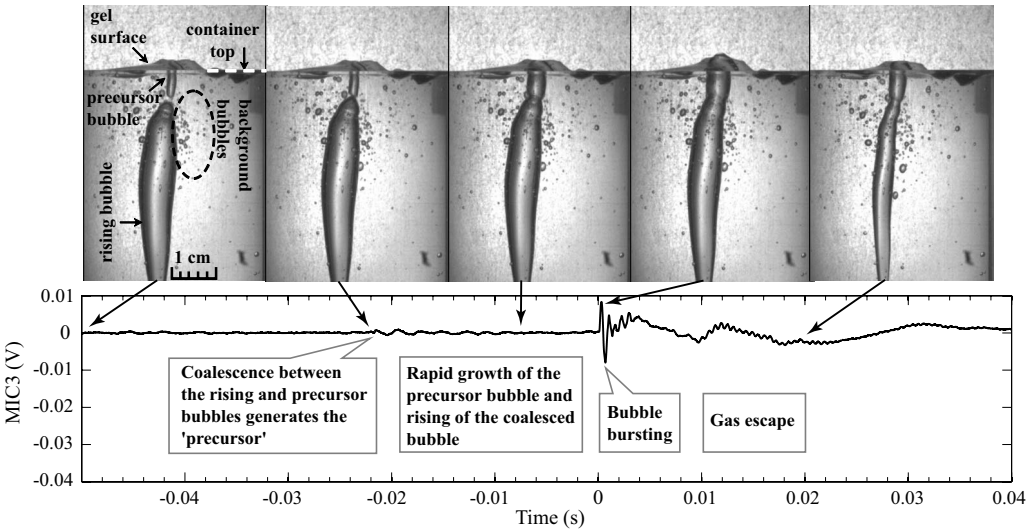

FIG. 8. Mechanism generating the precursor signal. A small bubble is trapped under the surface, due to previous bubble bursting. When the next bubble rises up, its coalescence with this small bubble generates the precursor acoustic signal. The subsequent acoustic waveform at bursting depends on the precursor time delay (see Fig. 3). Note that we display here the raw signal monitored by MIC3 (the jet component has not been removed yet).

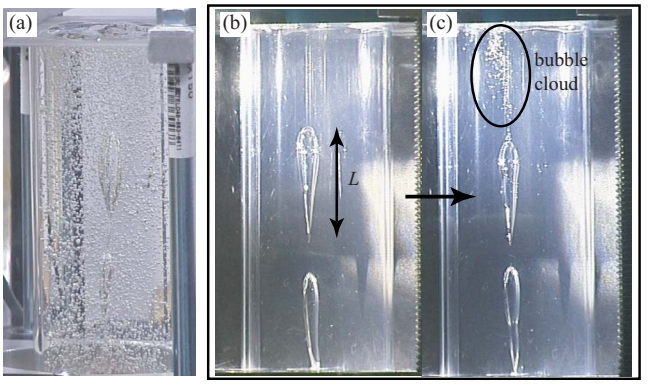

FIG. 9. (Color online) (a) Bubble rising through a gel-water mixture, initially filled with small trapped bubbles. (b) and (c) No modulation is observed for the first bubbles rising through the gel initially free of small background bubbles (b). After some time (c), a cloud composed of small trapped bubbles due to successive burstings forms beneath the surface. Modulation in the acoustic waveform and precursor time delay then appears.

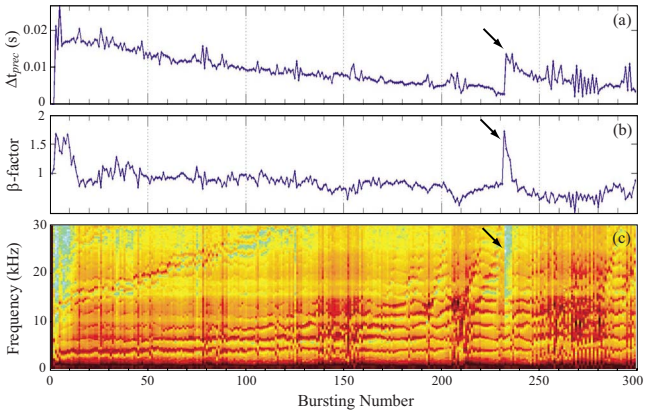

FIG. 10. (Color online) Pure gel experiment (no background bubbles). (a) Time-delay Δt_{prec} between the precursor and the acoustic signal associated with the bursting, (b) β factor (spectrum slope), and (c) normalized log-spectrogram of the bursting events, filtered between 0.78 and 29.9 kHz, as a function of the bursting event. Black arrows indicate the beginning of the modulation (see text).

By comparing Fig. 4(a) (Δt_{prec}) to Fig. 4(b) (β) and Fig. 4(d) (spectral peaks), we see that the variations in the precursor time delay are correlated with the variations in the β factor rather than with the peak variations. Figure 7 suggests that these variations are linked to the bubble bursting dynamics. Note that no correlation has been found between the size of the precursor bubble, and the precursor time delay.

C. Effect of the background bubbles

The fluid is initially filled with small trapped bubbles, due to the existence of a yield stress [Fig. 9(a)]. In order to investigate precisely the role of the precursor bubble on the waveform modulation, we performed a series of experiments starting from a gel at the same concentration, but initially free of bubbles [see Sec. II, and Fig. 9(b)]. Precursor bubbles are formed, as expected, after each bubble bursting, and coalesce with the following rising bubble to generate the precursor signal, as previously described in Sec. IV B. However, surprisingly, no clear modulation pattern is observed, either in the precursor time delay, the exponent β, or the acoustic waveform spectrogram (Fig. 10). Both the precursor time delay and the acoustic waveform vary very slowly in time, almost monotonically. Note, however, that the fluctuations superimposed to this monotonic behavior are correlated in the three graphs.

Modulation appears after more than 200 bubble burstings [black arrows in Figs. 10(a)–10(c)]. By this time, the small satellite bubbles generated by the successive burstings have formed a bubble cloud around the locus of bursting [Fig. 9(c)]. By this observation, we conclude that background bubbles play a crucial role in the existence of the modulation. We will discuss in the next section how they affect the fluid properties, and, hence, the dynamics of the system.

V. DISCUSSION

A. Modulation pattern

In order to generate a systematic modulation of the bursting behavior over a series of events, an internal evolution of the system is required. In other words, it requires the fluid, at a time t, to have the memory of the bursting history. Memory effects in a wide variety of non-Newtonian fluids have been previously reported in the literature. In particular, chaining of settling particles and coalescence of rising bubbles are common in viscoelastic fluids [35], although the physical processes responsible for these observations are not yet fully understood. In some fluids, normal stress difference effects [35,36] or successive stress creation and relaxation due to the passage of bubbles [26,37,38] have been invoked to explain this phenomenon. In shear-thinning fluids, it has been suggested that the passage of the leading bubble forms a corridor of reduced viscosity in its wake, through which the following bubble rises faster [37,39–41]. Since most complex fluids exhibit both elastic and shear-thinning properties, stress and viscosity effects are likely to be combined [42]. Different particle settling behaviors in fluids with and without an apparent yield stress point out that a change of the fluid microstructure itself, in addition to the effect of viscosity, is required to explain the observations [40]. In the present state of knowledge, the complexity in behavior exhibited by polymeric fluids prevents from an accurate description of the physical phenomena at stake in the memory effects. We will only refer, in this discussion, to a fluid *weakening* at the passage of a bubble, with a characteristic memory time.

In our system, the same precursor bubble and the above fluid layer, at the rupture point, are prompted during a certain number of bursting events. If the typical time between two bubbles is short enough for the fluid to keep the memory of the previous bursting, then the successive ruptures of the fluid layer at the surface lead to the weakening of the fluid around the rupture point at the surface. Consequently, the

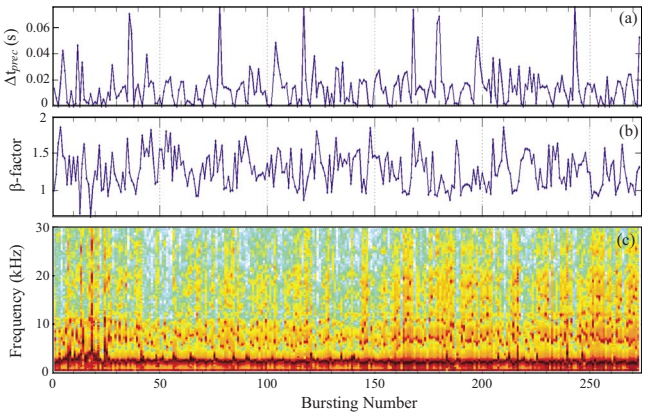

FIG. 11. (Color online) Experiment at smaller flux (0.07 mL/s), with bubbly gel. This experiment corresponds to the data displayed in Figs. 5(b) and 5(d). (a) Time-delay Δt_{prec} between the precursor and the bursting acoustic signal, (b) β factor, and (c) normalized log-spectrogram of the bursting events, filtered between 0.78 and 29.9 kHz, as a function of the bursting event. No clear modulation is observed.

time delay between the moment when the precursor bubble starts to be fed by the rising bubble and the subsequent bursting becomes shorter (Δt_{prec} decreases), and the characteristic time of the rupture process (surface opening) decreases. This process goes on until the fluid layer at the surface is weak enough to let the trapped precursor bubble escape; the fluid surface is then renewed. At this stage, both the precursor bubble and the rupture point are reset. Note that after the surface is renewed, when the following bubble bursts, the first hole tearing the film can form wherever on the bubble head, depending on the local stress, not always on its top. For this reason, the overpressurized air inside the bubble can escape from a different point. Consequently, the amplitude of the jet can strongly vary from one event to the other. This explains the amplitude difference between the events presented in Fig. 2 and Fig. 8, for instance, as well as our choice of two different angles for the microphone array (see Sec. II).

Figure 5 compares the correlation between Δt_{prec} and the β factor for two different fluxes (0.7 mL/s, Fig. 4, and 0.07 mL/s, Fig. 11). As previously commented in Sec. III B, for the higher flux (0.7 mL/s), we observe a clear correlation between the two parameters. For smaller flux, however, the time interval between two bubbles increases and this correlation is less obvious (Fig. 11) and tends to disappear [Fig. 5(b)]. This observation provides an estimate of the gel memory time, which is of the order of 10 s [Fig. 5(d)]. Note that in the experiment, sudden increase in Δt_{prec} and in β factor do not coincide, but the latter tends to be observed after one or two burstings (see Fig. 5). One explanation is that the precursor and the bursting signals may not be distinguishable when they are too close to each other. In this case, we might pick as a precursor the signal corresponding to a coalescence occurring deeper in the fluid column. This way, we artificially increase Δt_{prec}, before the time when the precursor bubble is reset.

The mechanism described above points out the importance of the succession of bubble burstings in generating the modulation. Experiments of a single bubble bursting have been performed with a precursor bubble injected manually below the free surface of the gel initially at rest. We then generated a bubble at the bottom of the experimental cell, and analyzed the interaction between this rising bubble and the trapped precursor bubble. The resulting acoustic signal is always resonant-type. Indeed, in these experimental conditions, no weakening of the gel properties below the surface occurs. Consequently, only resonant-type acoustic signals can be observed, without modulation.

B. Satellite bubbles

The series of experiments performed with a gel initially free of bubbles demonstrate the crucial role played by the satellite bubbles in the modulation. The formation of small, satellite bubbles by bubbling in a non-Newtonian fluid has been previously reported in the literature. In particular, it has been observed that background bubbles can be generated during continuous bubbling by either pinch-off at the nozzle [43,44], or coalescence of two bubbles in the bulk [45]. Moreover, in our experiments, in the process to obtain the pure gel, high pressure has been applied to the fluid to remove the small, remaining bubbles. As a consequence, the fluid may be oversaturated, and disturbance by bubble rising could cause satellite bubbles nucleation. However, in our experiments, the satellite bubbles are concentrated below the free surface (Fig. 9), and not all along the rising bubbles path. The above processes are, therefore, not the main responsible for the observable satellite bubbles generation. The bubble bursting is the most likely process to leave behind not only the precursor bubble (see Sec. IV B and Fig. 8), but also other millimetric or submillimetric bubbles. These satellite bubbles eventually form a bubble cloud [Fig. 9(c)], leading to the appearance of the acoustic waveform modulation.

Two possible mechanisms can account for the difference between the pure and bubbly gel for the modulation appearance. First, the presence of the satellite bubbles can affect significantly the rheological properties of the gel, and, therefore, the mechanism mentioned above. In order to test this possibility, we performed rheology measurements (see Appendix A). We find a history-dependence (Fig. 12), i.e., a gel memory effect [46,47]. In an attempt to quantify the memory accumulation in the experimental condition of the repetitive bubble rising and bursting, we performed a rheological simulation by imposing successive shear stress cycles to both the bubbly and the pure gel (Appendix B, Fig. 13). The imposed shear stress $\sigma = 100$ Pa is much above the yield stress ($\sigma_c \sim 30$ Pa for both the bubbly and pure gel, estimated from Fig. 12). However, we did not see any significant evolution of the fluid response over cycles either in the bubbly or in the pure gel, which we had expected to explain the modulation. The results of the rheology measurements clearly show that the satellite bubbles decrease the effective viscosity of the gel (Fig. 12) and, hence, strongly modify its dynamic response to a shear stress, i.e., a bubble rising (Fig. 13). This indicates that the satellite bubbles may be responsible for the precursor bubble to escape and be renewed more easily.

The second possible scenario considers the interaction between one or more satellite bubbles, and either the precursor

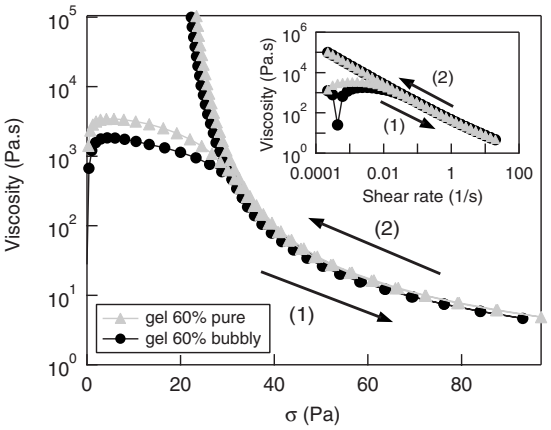

FIG. 12. Rheological properties of the gel 60%. Viscosity as a function of the shear stress (inset, as a function of shear rate) for the pure (no background bubble) and the bubbly (many background bubbles) gel. Experiments are performed from low to high (1), then high to low (2) shear rate (imposed shear rate, equilibration time $\Delta t = 10$ s).

bubble, or the rising bubble. This interaction could be responsible for renewing the rupture point and the precursor bubble, and, thus, for generating the modulation. No such evidence has been observed with the high-speed video camera; however, submillimetric bubbles are difficult to observe, and this hypothesis cannot be discarded.

C. Implication of repetitive phenomena

Although the mechanism generating the modulation has not been fully understood, this experiment demonstrates important aspects of repetitive phenomena. The modulation in the acoustic signal is generated by processes happening in the bulk. The fluid rheological properties and the presence of satellite bubbles—both features being linked together—play a crucial role in the existence of a modulation in the system. Understanding the signal temporal variations in repetitive phenomena can, therefore, provide information on the properties and dynamics of the system.

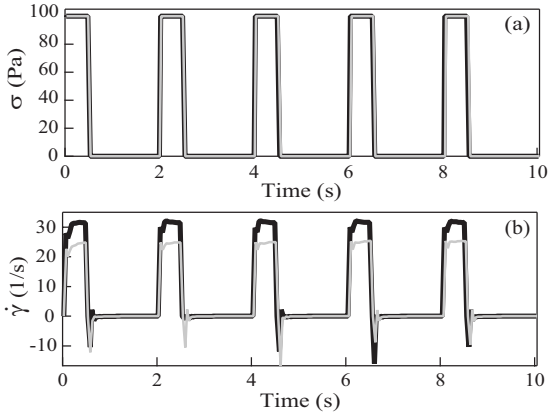

FIG. 13. Rheological simulation of in-line bubble interaction, in the gel 60%. (a) Imposed shear stress $\sigma = 100$ Pa for 0.5 s, then $\sigma = 0$ Pa for 1.5 s (five cycles). (b) Resulting shear rate $\dot{\gamma}$. (Gray line: pure gel; black line: bubbly gel.)

Volcanoes represent appealing systems where such understanding would be of crucial interest. Repetitive acoustic signals on volcanoes [3] display features similar to the ones observed in this study. For example, reported acoustic signals of continuous bubble bursting at Mount Erebus Volcano, Ross Island, Antarctica [4] or Karymsky volcano, Kamchatka [5] display harmonic spectra, as well as frequency gliding through time. On Soufrière Hills volcano, Montserrat island, slow changes of the seismic waveform [8] through time, and modulation in the ground tilt data are observed. Lava exhibits non-Newtonian behavior [48–50], including yield stress and memory effect [51]. The presence of small trapped bubbles inside the melt [16] and their coalescence with larger rising bubbles [7] strongly affect the magma rheology [16]. In such systems, investigating the acoustics of bubble bursting at the lava free surface provides a way to understand the physical processes controlling volcanic eruptions [7,16].

VI. CONCLUSION

We have reported here a simple experiment studying the acoustic signal emitted by a continuous bubbling in a non-Newtonian fluid. The bubble bursting generates an acoustic wave, generally audible (a few kHz). Due to the fluid rheological properties, the bubble walls remain still during the sound emission, and the bubble body acts as a resonator, excited by the film bursting. We point out the existence of a precursor acoustic signal, previous to each bubble bursting. The precursor signal is generated by the coalescence between the rising bubble and a small bubble that is left beneath the free surface after the previous bursting event, and trapped due to the fluid yield stress. The time-delay Δt_{prec} between the precursor signal and the bursting event is directly correlated with the waveform of the bursting signal. We also report a modulation of the acoustic signal at bursting, over a series of events. The waveform changes between a resonant-type and a blast-type signal, whose spectral contents vary both in the location of the frequency peaks and the general slope. We point out that the non-Newtonian fluid properties (memory effect) are responsible for this behavior.

We first inferred that the blast-type waveform is generated by an abrupt opening of the bubble and the resonance-type by a gradual opening, because the former is richer in the high-frequency components (smaller β factor) than the latter (larger β factor). However, this idea has not been confirmed by direct observations of the bubble bursting process. Some data show rather opposite tendency. The link between the waveform and the opening dynamics is more complex, and shall be the target of a future work. Nonetheless, it is important to underline that the results demonstrate that (1) the waveform generation in continuous bubble bursting is different from that generated by a single isolated bubble bursting, and (2) the preceding bubble bursting affects, via the precursor bubble, the subsequent bursting waveform. The link between the precursor bubble and the bursting dynamics also remains unknown at present.

The complex interaction between the background bubbles and the successive rising and bursting bubbles affects the

modulation, through both the fluid rheological properties, and the precursor generation. How these physical processes individually affect the global dynamics of the system still remains an open question. Additional experiments to investigate the exact influence of the fluid rheology, through systematic changes of the gel concentration, shall be the next step for this study.

Even if our laboratory-scale system does not claim at reproducing large-scale complex natural phenomena, it is interesting to point out the implications of such a study from a geophysical point of view. As discussed above, continuous changes in the acoustic waveform have been observed on volcanoes. At the laboratory scale, we point out that the change in the lava rheology, due to the presence of small trapped bubbles, may be responsible, alone, for the acoustic waveform evolution observed in repetitive events.

ACKNOWLEDGMENTS

This work was supported by JSPS Grant-in-Aid for Young Scientists (B) (Grant No. 20740251), and Office of International Earthquake and Volcano Research Promotion, ERI, University of Tokyo. J.-C. Géminard is acknowledged for helpful discussions. We thank two anonymous referees for greatly improving the manuscript with their comments.

APPENDIX A: RHEOLOGICAL PROPERTIES

The rheological properties of the fluid have been measured in the laboratory, with a BOHLIN C-VOR 150 rheometer, equipped with a plane-plane geometry (PP60, gap 1000 μm). Sand paper was glued to both upper and lower plates, in order to prevent any sliding at the walls. Temperature is kept constant through all the measurements ($T=25$ °C). Figure 12 displays the viscosity measurement, as a function of shear rate (or shear stress), for both the gel 60% with (bubbly gel) or without (pure gel) background bubbles. Measurements are performed from low to high shear rate, and then back from high to low shear rate. Note the hysteresis for small shear rate (shear stress) values. The fluid, with and without bubbles, is shear-thinning, and the presence of small trapped bubbles inside the material decreases its viscosity (Fig. 12).

APPENDIX B. RHEOLOGICAL SIMULATIONS

In order to mimic the passage of successive bubbles through the fluid, we realized the following experiments with the rheometer [25,38]. We impose to a sample of either pure, or bubbly gel, cycles of successive shear stress ($\sigma>0$) and rest ($\sigma=0$). The stress imposed by a single bubble rising through the fluid is of about $\rho g \phi_b \sim 100$ Pa, where $\rho=1000$ kg m^{-3} denotes the density of the fluid, $g=9.8$ m^2 s^{-1} the acceleration due to gravity, and $\phi_b \sim 1$ cm the typical bubble radius.

In the typical experimental series, presented in Fig. 3, for example, we measure the average time delay between two bubble burstings, $\langle \delta t_{\text{burst}} \rangle = 2.0 \pm 0.5$ s [see Fig. 5(c)]. The estimated time for a bubble shearing the surrounding fluid is about 0.5 s. We thus impose on the rheometer successive cycles of shear stress $\sigma=100$ Pa, during 0.5 s, followed by rest period ($\sigma=0$ Pa) of 1.5 s [Fig. 13(a)]. We measure the resulting shear rate $\dot{\gamma}$ [Fig. 13(b)]. For identical shear stress conditions [Fig. 13(a)], the pure and bubbly gel have a different response [Fig. 13(b)]. As expected from the viscosity measurements presented in Fig. 12, the pure gel presents a slightly higher viscosity, and thus, responds with a lower shear rate to the same stress condition.

Note in the first cycle that the gel, initially at rest, needs a longer time to reach the shear rate plateau than for the following cycles. Indeed, at rest, the polymer chains in the gel form a mesh, resisting the flow [52]. When imposing a shear stress above the yield stress σ_c (here, $\sigma_c \sim 30$ Pa), the time necessary to destructure the entangled chains introduces a delay in the gel flowing response. This effect is less important in the following cycles: the gel keeps the memory of the preshearing induced by the previous cycle. We find no evidence of the fluid aging—either for the pure or bubbly gel—through successive cycles of repetitive shear stress.

[1] M. Ichihara, T. Yanagisawa, Y. Yamagishi, H. Ichikawa, and K. Kurita, Japan Earth and Planetary Science Joint Meeting (2005), Abstract No. A111-P004.
[2] S. E. Ingebritsen and S. A. Rojstaczer, J. Geophys. Res. **101**, 21891 (1996).
[3] M. Ripepe, P. Poggi, T. Braun, and E. Gordeev, Geophys. Res. Lett. **23**, 181 (1996).
[4] C. A. Rowe, R. C. Aster, P. R. Kyle, R. R. Dibble, and J. W. Schlue, J. Volcanol. Geotherm. Res. **101**, 105 (2000).
[5] J. B. Johnson, R. C. Aster, M. C. Ruiz, S. D. Malone, P. J. McChesney, J. M. Lees, and P. R. Kyle, J. Volcanol. Geotherm. Res. **121**, 15 (2003).
[6] B. Voight, R. P. Hoblitt, A. B. Clarke, A. B. Lockhart, A. D. Miller, L. Lynch, and J. McMahon, Geophys. Res. Lett. **25**, 3405 (1998).
[7] E. A. Parfitt, J. Volcanol. Geotherm. Res. **134**, 77 (2004).
[8] D. N. Green and J. Neuberg, J. Volcanol. Geotherm. Res. **153**, 51 (2006).
[9] D. N. Green and D. Bowers, Seismol. Res. Lett. **79**, 546 (2008).
[10] W. Müller and J.-M. di Meglio, J. Phys.: Condens. Matter **11**, L209 (1999).
[11] D. Weaire and S. Hutzler, *The Physics of Foams* (Clarendon Press, Oxford, 1999).
[12] N. Vandewalle, J. F. Lentz, S. Dorbolo, and F. Brisbois, Phys. Rev. Lett. **86**, 179 (2001).
[13] N. Vandewalle and J. F. Lentz, Phys. Rev. E **64**, 021507 (2001).
[14] N. Vandewalle, H. Caps, and S. Dorbolo, Physica A **314**, 320 (2002).

[15] J. Ding, F. W. Tsaur, A. Lips, and A. Akay, Phys. Rev. E **75**, 041601 (2007).
[16] H. M. Gonnermann and M. Manga, Annu. Rev. Fluid Mech. **39**, 321 (2007).
[17] R. P. Chhabra, *Bubbles, Drops and Particles in non-Newtonian Fluids*, 2nd ed., Chemical Industries (Taylor & Francis, London, 2007), Series No. 113.
[18] T. Divoux, V. Vidal, F. Melo, and J.-C. Géminard, Phys. Rev. E **77**, 056310 (2008).
[19] R. B. Bird, R. C. Armstrong, and O. Hassager, *Dynamics of Polymeric Liquids* (Wiley, New York, 1987), Vols. I and II.
[20] A. Belmonte, Rheol. Acta **39**, 554 (2000).
[21] N. Z. Handzy and A. Belmonte, Phys. Rev. Lett. **92**, 124501 (2004).
[22] V. Vidal, J.-C. Géminard, T. Divoux, and F. Melo, Eur. Phys. J. B **54**, 321 (2006).
[23] H. Z. Li, X. Frank, D. Funfschilling, and Y. Mouline, Chem. Eng. Sci. **56**, 6419 (2001).
[24] T. J. Lin and G.-M. Lin, Can. J. Chem. Eng. **81**, 476 (2003).
[25] H. Z. Li, X. Frank, D. Funfschilling, and P. Diard, Phys. Lett. A **325**, 43 (2004).
[26] T. Divoux, E. Bertin, V. Vidal, and J.-C. Géminard, Phys. Rev. E **79**, 056204 (2009).
[27] H. Z. Li, Y. Mouline, L. Choplin, and N. Midoux, Int. J. Multiphase Flow **23**, 713 (1997).
[28] N. Dubash, and I. A. Frigaard, J. Non-Newtonian Fluid Mech. **142**, 123 (2007).
[29] R. D. Ayers, L. J. Eliason, and D. Mahgerefteh, Am. J. Phys. **53**, 528 (1985).
[30] J. Kemp, Ph.D. thesis, University of Edinburgh, 2002 (unpublished).
[31] J. W. S. Rayleigh, *The Theory of Sound* (Dover, New York, 1945), Vols. I and II.
[32] L. E. Kinsler, A. R. Frey, A. B. Coppens, and J. V. Sanders, *Fundamentals of Acoustics*, 3rd ed. (Wiley, New York, 1982),
[33] H. Levine and J. Schwinger, Phys. Rev. **73**, 383 (1948).
[34] A. Pierce, *Acoustics—An Introduction to Its Physical Principles and Applications* (ASA, New York, 1989).
[35] J. Michele, R. Pätzold, and R. Donis, Rheol. Acta **16**, 317 (1977).
[36] D. D. Joseph, Y. J. Liu, M. Poletto, and J. Feng, J. Non-Newtonian Fluid Mech. **54**, 45 (1994).
[37] X. Frank, H. Z. Li, and D. Funfschilling, Eur. Phys. J. E **16**, 29 (2005).
[38] H. Z. Li, Y. Mouline, D. Funfschilling, P. Marchal, L. Choplin, and N. Midoux, Chem. Eng. Sci. **53**, 2219 (1998).
[39] M. J. Riddle, C. Narvaez, and R. B. Byrd, J. Non-Newtonian Fluid Mech. **2**, 23 (1977).
[40] G. Gheissary and B. H. A. A. van den Brule, J. Non-Newtonian Fluid Mech. **67**, 1 (1996).
[41] S. Daugan, L. Talini, B. Herzhaft, and C. Allain, Eur. Phys. J. E **7**, 73 (2002).
[42] Z. Yu, A. Wachs, and Y. Pesson, J. Non-Newtonian Fluid Mech. **136**, 126 (2006).
[43] S. T. Thoroddsen, T. G. Etoh, and K. Takehara, Phys. Fluids **19**, 042101 (2007).
[44] J. C. Burton and P. Taborek, Phys. Rev. Lett. **101**, 214502 (2008).
[45] F. H. Zhang and S. T. Thoroddsen, Phys. Fluids **20**, 022104 (2008).
[46] J. Mewis, J. Non-Newtonian Fluid Mech. **6**, 1 (1979).
[47] H. A. Barnes, J. Non-Newtonian Fluid Mech. **70**, 1 (1997).
[48] S. L. Webb and D. B. Dingwell, J. Geophys. Res. **95**, 15695 (1990).
[49] L. Caricchi, L. Burlini, P. Ulmer, T. Gerya, M. Vassalli, and P. Papale, Earth Planet. Sci. Lett. **264**, 402 (2007).
[50] Y. Lavallée, P. G. Meredith, D. B. Dingwell, K.-U. Hess, J. Wassermann, B. Cordonnier, A. Gerik, and J. H. Kruhl, Nature (London) **453**, 507 (2008).
[51] H. Pinkerton and G. Norton, J. Volcanol. Geotherm. Res. **68**, 307 (1995).
[52] P. C. F. Møller, J. Mewis, and D. Bonn, Soft Matter **2**, 274 (2006).